Uncertainty Analysis in Airfoil-Turbulence Interaction Noise Using Polynomial Chaos Expansion

Jamie Kha *
University of Technology Sydney, Sydney, NSW 2000, Australia

Paul Croaker †
Defence Science and Technology Group, Melbourne, VIC 3000, Australia

Mahmoud Karimi ‡
University of Technology Sydney, Sydney, NSW 2000, Australia

Alex Skvortsov §
Defence Science and Technology Group, Melbourne, VIC 3000, Australia

Airfoil-turbulence interaction noise is a known source of environmental disturbance and acoustic performance loss in aeroacoustics and hydroacoustics. This noise can be predicted using semi-analytical models that require input measurements of the incoming turbulent flow parameters. However, the turbulence parameters are inherently difficult to measure accurately. These parameters, which include the turbulence kinetic energy and its dissipation rate, have a stochastic nature. This study aims to investigate how small variations in the measurements of turbulence parameters affect the uncertainty of the predicted airfoil-turbulence interaction noise. This is achieved by applying polynomial chaos expansion (PCE) to the semi-analytical model of Amiet's theory for airfoil-interaction noise. The validity of the deterministic and stochastic simulations is ensured by comparisons against available experimental data from the literature, and Monte Carlo simulations, respectively. Uncertainty quantification is then performed using a stochastic collocation technique, where the aerodynamic noise is evaluated at specific collocation points to estimate the coefficients required for PCE. Both the individual and combined effects of varying the uncertain input turbulence parameters are simulated to quantify the uncertainty of the output aerodynamic noise. The insights gained from the results suggest it is important to incorporate the stochastic behavior of the incoming turbulent flow in operational models for airfoil-turbulence interaction noise predictions.

*PhD Candidate, School of Mechanical and Mechatronic Engineering, jamie.kha@student.uts.edu.au
†Discipline Lead Cavitation and Unsteady Flow, Platforms Division
‡Senior Lecturer, School of Mechanical and Mechatronic Engineering
§Principal Scientist, Platforms Division

Nomenclature

b = Airfoil semi-chord, m

c = Airfoil chord, m

C_∞ = Speed of sound in air, $\mathrm{m{\cdot}s^{-1}}$

d = Airfoil half-span, m

f = Frequency, $\mathrm{s^{-1}}$

k = Wavenumber, $\mathrm{m^{-1}}$

k_e = Characteristic wavenumber of energy-containing eddies $\mathrm{m^{-1}}$

k_x = Chordwise wavenumber $\mathrm{m^{-1}}$

k_y = spanwise wavenumber $\mathrm{m^{-1}}$

K_y = spanwise specific wavenumber

u' = Velocity fluctuation root-mean-square, $\mathrm{m{\cdot}s^{-1}}$

U = Free stream air speed, $\mathrm{m{\cdot}s^{-1}}$

U_c = Convection air speed, $\mathrm{m{\cdot}s^{-1}}$

M = Mach number

β = Compressibility factor

ρ_0 = Airflow density, $\mathrm{kg{\cdot}m^{-3}}$

ω = Angular frequency, $\mathrm{rad{\cdot}s^{-1}}$

κ = Turbulence kinetic energy, $\mathrm{m^2s^{-2}}$

ε = Turbulence kinetic energy dissipation rate, $\mathrm{m^2s^{-3}}$

Λ_f = Turbulence integral length scale

I. Introduction

Aerodynamic noise is a significant health concern to society, and managing the noise levels produced by aerostructures is an ongoing engineering issue [1–3]. Generally, industries related to wind farm technologies and aircraft manufacturing for commercial airline services are the most impacted. These industries must design suitable aerostructures to meet specific noise regulations. For example, such designs can involve modifications to the leading edge and trailing edge of the airfoil geometry, which has been shown to assist with noise reduction [4–6]. Validation of these new designs necessitates accurately predicting the noise radiated to the environment. While significant advancements in predicting noise levels from airfoil-turbulence interactions are reported in the literature [7], the consistent difficulty is to accurately measure incoming turbulent flow with the current experimentation and numerical approaches [8]. The accuracy of predictions compared with real-world specifications can vary significantly due to the stochastic nature of turbulence.

Understanding the variations in predictions will be integral for future compliance of aerostructures with noise regulations. Therefore, the application of uncertainty quantification (UQ) is suggested. In the literature, UQ is applied to engineering systems to deliver insight into the associated input-output relationship [9–18]. However, minimal studies have used stochastic analysis in the field of aeroacoustics. This is especially important as the modern theory of turbulence now incorporates the statistics of the driving parameters, the turbulence kinetic energy and dissipation rate [19]. This refinement to how turbulence is described can significantly change the statistics of turbulent fluctuations, leading to the well-known phenomenon of intermittency [19, 20]. This implies that prediction models that are based only on mean parameters of turbulent flow should be re-evaluated and modified.

Turbulence is characterized by a random and chaotic distribution of velocity fluctuations of a broad range of scales. This distribution lends itself to a statistical representation, with the parameters often represented by quantities such as turbulence kinetic energy and dissipation rate. For a given flow, these turbulence quantities are typically expressed as mean values, with these mean values used in the subsequent analysis of turbulence ingestion noise. However, evidence has shown that both the turbulence kinetic energy and turbulence dissipation rate have random natures themselves, resulting in the well-known phenomenon of intermittency of turbulence, which strongly influences other statistics of turbulence flow [21]. When studying the sound produced by airfoil-turbulence interaction, a classical approach pioneered by Amiet [22] involves decomposing the turbulence distribution of scales into an ensemble of discrete, uncorrelated wavenumbers. The interaction of these discrete wavenumber fluctuations with the airfoil and the resulting acoustic radiation is then calculated by combining the gust response of an infinitely thin airfoil with Curle's analogy [23]. Related techniques of backscattering correction from Roger and Moreau have also been developed [24]. These techniques have produced reasonable estimates of the mean far-field sound produced by airfoil-turbulence interaction noise [25]. Due to the stochastic nature of turbulence, both the turbulence kinetic energy and dissipation rate fluctuate around the mean, and this may have a significant influence on the generated sound. This necessitates an investigation of the effect of statistical variation in the turbulence spectrum on airfoil-turbulence interaction noise so that predictions can better represent and include the stochastic nature involved. Techniques relating to uncertainty analysis can be employed in these situations.

Uncertainty quantification has been used in engineering applications to quantify the effect of small variations in the inputs on the output uncertainty [9–18]. This is especially important when the sensitivity of measurements can result in significant changes to the prediction. How the uncertainty of turbulence parameter measurements will impact the output noise may indicate that the process of designing aerostructures to accommodate noise regulations may need reconsideration, or the noise regulation itself may need to be changed to accommodate for uncertainty. Various methods have been devised to understand an input-output relationship by using statistical models to describe uncertainty. Two common UQ methods include Monte Carlo simulation (MCS) and polynomial chaos expansion (PCE) [26–28]. MCS is a traditional random sampling method of quantifying uncertainty. PCE is a non-sampling method for quantifying uncertainty by expressing inputs and outputs as polynomials. These methods are favored in literature due to their relative

ease of implementation and effectiveness [29]. In aeroacoustics, there have been efforts of UQ applied in trailing edge noise where uncertainty in the trailing edge noise predictions was examined using MCS and stochastic collocation (via PCE) [9]. It was found that the stochastic collocation framework is two orders of magnitude more efficient than MCS in achieving the same accuracy. This is an important advantage that PCE has over traditional sampling methods. Polynomial chaos expansion and the stochastic collocation framework are more computationally efficient than MCS. From the trailing edge noise results, it was found that there is significant variance associated with noise predictions. In another work [30], UQ is applied to the leading edge of an airfoil, with the analysis focused on the force induced by the airfoil-turbulence interaction. The airfoil was modeled with the finite element method, and the theory of Sears was used to predict the gust response function. PCE was employed to model the uncertainty of several input parameters to study the airfoil gust response. These parameters included the turbulence integral length scale, the streamwise velocity fluctuations, and the damping in the structure. The method allows visualization of the response distribution and informs future designs of the variations in a structure's response due to uncertainty of the input parameters. It is inferred from the literature, which spans a wide range of applications, that UQ is useful, especially in describing physical problems with statistical behaviors. UQ enables more informed engineering choices based on the sensitivity of prediction models.

The novelty of the present work is in investigating the effect of the uncertainty in turbulence parameters on the aerodynamic noise generated by the airfoil-turbulence interaction. Aerodynamic noise is modeled by the semi-analytical approach of Amiet's theory. With this model, the deterministic prediction of airfoil-turbulence interaction noise is generated and verified against corresponding results presented by Santana [25]. A stochastic collocation-based technique is then used to calculate the PCE for the airfoil-turbulence noise. Far-field noise, characterized as a sound pressure level, is evaluated only at so-called collocation points, and the coefficients for the PCE are estimated based on these responses. Motivated by K62 [31], the uncertain input parameters of the turbulence flow, which include the kinetic energy and dissipation rate, are assumed to follow a lognormal probability distribution function (PDF) to capture its statistical variation. Results are then generated from the PCE, and the effects of the individual and combined uncertain input parameters from the incoming turbulent flow on the airfoil-turbulence interaction noise are examined. It is demonstrated from these results that there is a significant influence on the output noise uncertainty from small variations in the input parameters. To verify the results from PCE, the alternative Monte Carlo simulation approach is employed to generate corresponding results. The proposed mathematical approach provides an efficient tool for quantifying the uncertainty of leading edge noise from the variations in turbulence parameters.

The contents of the paper are as follows. In Section II, the analytical scattering model of Amiet's theory is described, followed by a discussion on the upwash velocity spectrum, which embeds the turbulence characteristics into the physical problem, and finally, a description of how uncertainty quantification is employed in the study. Section III demonstrates results from the PCE and MCS for the individual and combined influence of the turbulence parameters. Finally, in Section IV, the conclusions of the investigation are summarized.

II. Problem statement

This section details the theoretical components necessary to analyze the uncertainty in airfoil-turbulence interaction noise from the leading edge of an airfoil from the stochastics of the input turbulent flow. First, the scattering model applied to model the aeroacoustic system of an airfoil-turbulence interaction is described. Second, adjustments to the upwash velocity spectrum via RDT are discussed to better model the physical interaction of the airfoil and incoming turbulent flow. And finally, a description of the uncertainty quantification technique applied to extract the output uncertainty of the noise is presented.

A. Scattering model

Aerodynamic noise, which is the noise produced via pressure fluctuations from flow over structures such as propellers, airfoils, and airframes, is the main focus of this study, and more specifically, the analysis of the leading edge noise of an airfoil. An airfoil subject to incoming turbulence flow will develop lift fluctuations over its surface and consequently radiate noise to the far field as acoustic dipoles. Typically the turbulence flow field is caused by distortions and other aerodynamic elements upstream of the airfoil. A schematic diagram of the airfoil-turbulence interaction noise system is shown in Figure 1. The input parameters influencing leading edge noise are turbulence parameters, including turbulence intensity and turbulence integral length scale. These parameters are measured by experimentation or high-fidelity computational fluid dynamics (CFD) simulations. Collecting accurate values of these parameters remains a challenging task due to the sensitive nature of the system. As such, predictions of the radiated noise may significantly vary due to small variations of turbulence parameters. It is herein recognized that there is an opportunity to better understand aerodynamic noise by studying the effect of uncertainty of turbulence parameters on predicting output noise. By quantifying output uncertainty, confidence in predictions made to leading-edge noise production due to airfoil-turbulence interactions can more reasonably be justified.

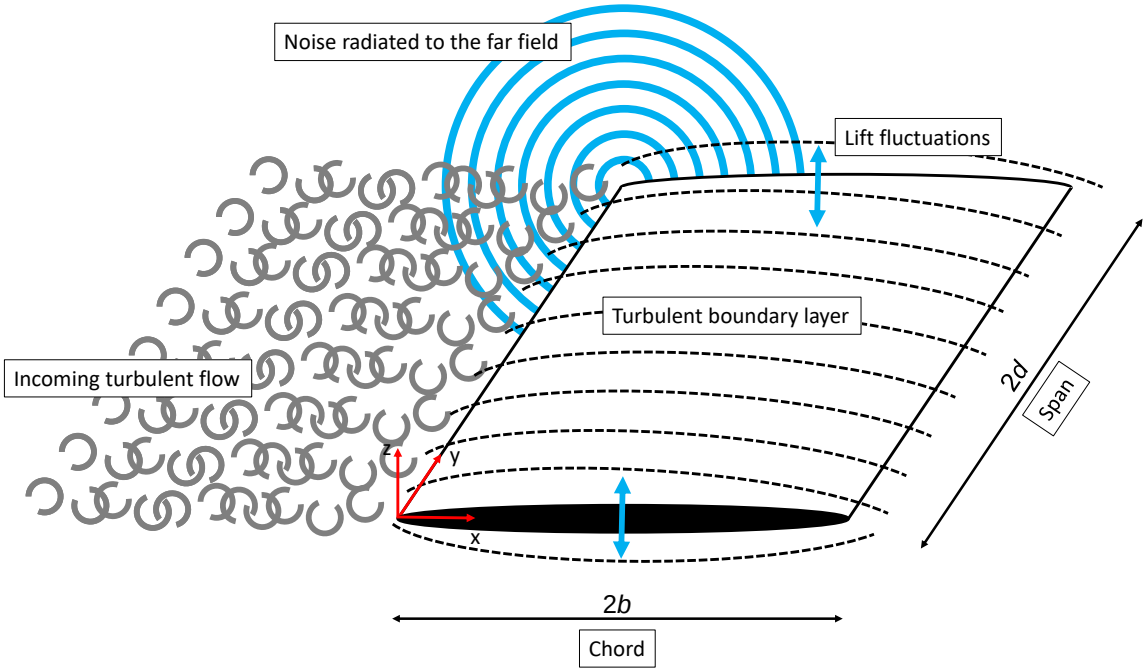

Fig. 1 Noise generation by airfoil-turbulence interaction noise

The leading edge noise is modeled using the analytical scattering model from Amiet's theory [22]. From this model, the power spectral density (PSD) of the far-field sound can be calculated with the following [32]:

$$S_{pp}\left(x,y,z,\omega\right)=\left(\frac{\rho_0 zkb}{\sigma_0^2}\right)^2\pi Ud\int_{-\infty}^{\infty}\frac{\sin^2\left[\left(K_y-k_y\right)d\right]}{\pi d\left(K_y-k_y\right)^2}\phi_{ww}\left(K_x,k_y\right)\left|\mathcal{L}\left(x,y,z,K_x,k_y\right)\right|^2\mathrm{d}k_y\,, \tag{1}$$

where ρ_0 is the airflow density, k is the acoustic wavenumber, b is the airfoil semi-chord, d is the airfoil half-span, U is the free stream air speed, k_x is the chordwise wavenumber, k_y is the spanwise wavenumber, $K_y=ky/\sigma_0$ is the spanwise specific wavenumber, $\sigma_0=\sqrt{x^2+\beta^2\left(y^2+z^2\right)}$ is the distance between the source (located at the origin) and listener position (x,y,z) considering convective effects, $M=u/C_\infty$, $\beta=\sqrt{1-M^2}$, $f=kC_\infty/2\pi$, $\omega=2\pi f$, ϕ_{ww} is the upwash velocity spectrum, and $\mathcal{L}$ is the aeroacoustic transfer function. The aeroacoustic transfer function, $\mathcal{L}=\mathcal{L}_1+\mathcal{L}_2$, is a sum of contributions from the primary scattering of incoming turbulence at the leading edge ($\mathcal{L}_1$) and back-scattering corrections [24] at the trailing edge ($\mathcal{L}_2$) respectively. The reader is advised to follow the derivations in Ref. [33] to obtain expressions for the aeroacoustic transfer functions. For supercritical gusts $\gamma^2<0\Rightarrow\bar{k}_y<\mu\beta$, the aeroacoustic transfer functions are defined as [34]

$$\mathcal{L}_1^{\mathrm{sup}}\left(x,y,z,k_x,k_y\right)=\frac{1}{\pi}\sqrt{\frac{2}{\left(\bar{k}_x+\beta^2\gamma\right)\theta_1}}E^*\left(2\theta_1\right)\mathrm{e}^{\mathrm{i}\theta_2}\,, \tag{2}$$

$$\mathcal{L}_2^{\sup}\left(x, y, z, k_x, k_y\right) \simeq \frac{\mathrm{e}^{\mathrm{i}\theta_2}}{\pi\theta_1\sqrt{2\pi\left(\bar{k}_x+\beta^2\gamma\right)}}$$
$$\left\{\mathrm{i}\left(1-\mathrm{e}^{-2\mathrm{i}\theta_1}\right)+(1-\mathrm{i})\left[E^*\left(4\gamma\right)-\sqrt{\frac{2\gamma}{\theta_3}}\mathrm{e}^{-2\mathrm{i}\theta_1}E^*\left(2\theta_3\right)\right]\right\}, \tag{3}$$

with $\theta_1=\gamma-\mu x/\sigma_0$, $\theta_2=\mu\left(M-x/\sigma_0\right)-\pi/4$, $\theta_3=\gamma+\mu x/\sigma_0$, $\gamma^2=\mu^2-\bar{k}_y^2/\beta^2$, $\mu=\bar{k}_x M/\beta^2$ and E^* is an expression containing Fresnel integrals.

$$E^*\left(r\right)=C_2\left(r\right)-\mathrm{i}S_2\left(r\right)=C\left(\sqrt{\frac{2}{\pi}r}\right)-\mathrm{i}S\left(\sqrt{\frac{2}{\pi}r}\right), \tag{4}$$

where $C\left(r\right)=\int_0^r\cos\left(t^2\right)\mathrm{d}t$ and $S\left(r\right)=\int_0^r\sin\left(t^2\right)\mathrm{d}t$. While for subcritical gusts $\gamma^2>0\Rightarrow\bar{k}_y\geq\mu\beta$, the following expressions are derived from Ref. [33] as corrections to Rozenberg's expressions [35]

$$\mathcal{L}_1^{\mathrm{sub}}\left(x, y, z, k_x, k_y\right)=\frac{1}{\pi\sqrt{\gamma'\beta^2+\mathrm{i}\bar{k}_x}}\mathrm{e}^{\mathrm{i}\mu\left(M-x/\sigma\right)}\frac{1}{\sqrt{\theta}}\mathrm{e}^{-\mathrm{i}\pi/4}\mathrm{erf}\left(\sqrt{2\mathrm{i}\theta}\right), \tag{5}$$

$$\mathcal{L}_2^{\mathrm{sub}}\left(x, y, z, k_x, k_y\right)=-\frac{\mathrm{e}^{\mathrm{i}\mu\left(M-x/\sigma\right)}}{\pi\sqrt{2\pi\left(\gamma'\beta^2+\mathrm{i}\bar{k}_x\right)}}\frac{1}{\gamma'-\mathrm{i}\mu x/\sigma}$$
$$\left\{\left[1-\mathrm{erf}\left(\sqrt{4\gamma'}\right)\right]-\mathrm{e}^{-2\left(\gamma'-\mathrm{i}\mu x/\sigma\right)}+\left[\sqrt{2\gamma'}\frac{\mathrm{e}^{-2\left(\gamma'-\mathrm{i}\mu x/\sigma\right)}}{\sqrt{\gamma'+\mathrm{i}\mu x/\sigma}}\mathrm{erf}\left(\sqrt{2\left(\gamma'+\mathrm{i}\mu x/\sigma\right)}\right)\right]\right\}, \tag{6}$$

with $\theta=-\left(\frac{\mu x}{\sigma}+\mathrm{i}\gamma'\right)$, $\gamma'^2=-\gamma^2$, and $\mathrm{erf}\left(Z\right)$ is the complex error function that is related to the Fresnel integrals by $\mathrm{erf}\left(Z\right)=(1+\mathrm{i})\,E^*\left(-\mathrm{i}Z^2\right)$. It is known that the Fresnel integrals can be approximated by rational polynomials [36]

$$C\left(r\right)\simeq 0.5+f\left(r\right)\sin\left(\frac{\pi}{2}r^2\right)-g\left(r\right)\cos\left(\frac{\pi}{2}r^2\right), \tag{7}$$

$$S\left(r\right)\simeq 0.5-f\left(r\right)\cos\left(\frac{\pi}{2}r^2\right)-g\left(r\right)\sin\left(\frac{\pi}{2}r^2\right), \tag{8}$$

for $r\in(0,\infty)$, where $f\left(r\right)=\left(1+0.926r\right)/\left(2+1.792r+3.104r^2\right)$ and $g\left(r\right)=1/\left(2+4.142r+3.492r^2+6.670r^3\right)$. By using this approximation, there is a significant runtime improvement to the numerical simulation. The PSD of the airfoil-turbulence interaction noise is presented as a sound pressure level (SPL) in the units of dB/Hz [25, 37, 38]

$$\mathrm{SPL}=10\log_{10}\left(\frac{S_{pp}}{p_{\mathrm{ref}}^2}\right)\text{ where }p_{\mathrm{ref}}=2\times10^{-5}\ \text{Pa}. \tag{9}$$

The final component of the PSD is the upwash velocity spectrum which is described in the next section.

B. Upwash velocity spectrum

Isotropic turbulence is commonly modeled using the von Kármán and Liepmann energy spectrum models. Using the energy spectrum, the upwash velocity spectrum can then be derived. For the Liepmann spectrum, the energy spectrum is given as [39]

$$E\left(k\right) = \frac{8}{\pi} u'^2 \Lambda_f \frac{\Lambda_f^4 k^4}{\left(1 + \Lambda_f^2 k^2\right)^3}, \tag{10}$$

where u' is the velocity fluctuation root-mean-square and Λ_f is the turbulence integral length scale. The corresponding upwash velocity spectrum is then found to be

$$\phi_{\mathrm{ww}}\left(k_x, k_y\right) = \frac{3u'^2}{4\pi} \Lambda_f^2 \frac{\Lambda_f^2 \left(k_x^2 + k_y^2\right)}{\left[1 + \Lambda_f^2 \left(k_x^2 + k_y^2\right)\right]^{5/2}}. \tag{11}$$

While the von Kármán spectrum is given as [39]

$$E\left(k\right) = \frac{55}{9} \frac{\Gamma\left(5/6\right)}{\sqrt{\pi}\Gamma\left(1/3\right)} \frac{u'^2}{k_e} \frac{\left(k/k_e\right)^4}{\left[1 + \left(k/k_e\right)^2\right]^{17/6}}, \tag{12}$$

where k_e is the characteristic wavenumber of energy-containing eddies. The corresponding upwash velocity spectrum is then found to be

$$\phi_{\mathrm{ww}}\left(k_x, k_y\right) = \frac{4}{9\pi} \frac{u'^2}{k_e^2} \frac{\hat{k}_x^2 + \hat{k}_y^2}{\left(1 + \hat{k}_x^2 + \hat{k}_y^2\right)^{7/3}}. \tag{13}$$

It is noticed by Hunt [40] that if the turbulent flow is over a boundary, then the energy spectrum will more accurately follow a proportionality of $k^{-10/3}$ due to the rapid distortion theory from Batchelor [41]. At high frequencies, the decay no longer follows a $-5/3$ rule but rather a $-10/3$ asymptote. This modification is applied to the energy spectrum by exchanging the exponent from $17/6$ to $22/6$ to account for the anisotropic distorted scenario. When this modification is applied to the von Kármán spectrum, the upwash velocity spectrum is derived to be

$$\phi_{ww}\left(k_x, k_y\right) = \frac{91}{36\pi} \frac{u'^2}{k_e^2} \frac{\hat{k}_x^2 + \hat{k}_y^2}{\left(1 + \hat{k}_x^2 + \hat{k}_y^2\right)^{19/6}}, \tag{14}$$

with $k_x \rightarrow K_x = \omega/U_c$ where $U_c = 0.8U$, $\bar{k}_i = k_i b$ is the normalized wavenumber, $\mu = \bar{k}_x M/\beta^2$, $k_e = \sqrt{\pi}\Gamma\left(5/6\right)/\left(\Lambda_f \Gamma\left(1/3\right)\right)$ where $\Gamma\left(r\right) = \int_0^\infty \mathrm{e}^{-t} t^{r-1} \mathrm{d}t$ is the Gamma function, and $\hat{k}_i = k_i/k_e$. Implementing this upwash velocity spectrum into the Eq 1 along with the aeroacoustic transfer functions from Eqs 2, 3, 5, 6 enables the integral to be evaluated. Next will be implementing the PCE method to the SPL prediction from Amiet's theory.

C. Uncertainty quantification

The mean values of the turbulence parameters, $\bar{T} = \{\bar{\kappa}, \bar{\varepsilon}\}$ are assumed to be constant and are related to the experimental measurements of flow quantities as follows

$$\bar{\kappa} = \frac{3}{2}u'^2, \tag{15}$$

$$\bar{\varepsilon} = 0.39\frac{\bar{\kappa}^{\frac{3}{2}}}{\Lambda_f}, \tag{16}$$

$$k_e = 1.9\frac{\varepsilon}{\kappa^{\frac{3}{2}}}. \tag{17}$$

The present study utilizes two-parameter models. Two-parameter PDFs include the lognormal distribution and normal distribution. The lognormal distribution is expressed as an exponential of the normal distribution

$$T = \{\kappa, \epsilon\} \sim \mathcal{LN}\left(M, S^2\right) \text{ or } \log(T) \sim \mathcal{N}\left(M_N, S_N^2\right), \tag{18}$$

where M, S is the mean and standard deviation of the lognormal distribution, respectively and M_N, S_N is the mean and standard deviation of the normal distribution, respectively. The normal distribution is expressed as

$$T = \{\kappa, \epsilon\} \sim \mathcal{N}\left(M_N, S_N^2\right), f\left(x; M_N, S_N^2\right) = \frac{1}{\sqrt{2\pi S_N^2}} \mathrm{e}^{-\frac{(x-M_N)^2}{2S_N^2}}, \tag{19}$$

where $M_N = \log\left(\frac{M^2}{\sqrt{S^2+M^2}}\right)$ and $S_N = \sqrt{\log\left(\frac{S^2}{M^2}+1\right)}$. To introduce variation into the input parameters, a metric known as the coefficient of variation (CV) where CV = standard deviation / mean, is used to quantify the uncertainty. This metric is used for distributions that consist of only positive values as in the case of the present study. When the mean is zero, the metric becomes inadequate for use in uncertainty analysis. In this study, the phenomenon of turbulence is considered, and therefore, its input parameters are never zero and always positive. The present study focuses on low variance and limits the CV to 0.15 when applying polynomial chaos expansion and the Monte Carlo method.

1. Polynomial Chaos Expansion

Polynomial chaos expansion is applied to the system to investigate the effect of small input variations on the output sound pressure level. The sound pressure level is calculated using input turbulence parameters. Experimental measurements of turbulence flow quantities, turbulence integral length scale $\left(\Lambda_f\right)$ and turbulence intensity (u'/U), are transformed into a new set of turbulence parameters ($T = \{\kappa, \epsilon\}$): turbulence kinetic energy (κ) and turbulence kinetic energy dissipation rate (ε). Uncertainty is introduced by varying the input turbulence parameters based on a chosen

probability distribution function (PDF). Input variation can then be summarized as

$$T = \{\kappa, \epsilon\} \sim \text{PDF (parameter1,parameter2).}$$

Polynomial chaos expansion is utilized to approximate PDFs using a sum of polynomials. The input parameters T are formulated as a sum of polynomials

$$T = \sum_{i=0}^{N} t_i \Psi_i \left(\boldsymbol{\xi}\right), \tag{20}$$

where t_i are the coefficients, Ψ_i are stochastic basis functions (polynomials), and $\boldsymbol{\xi}$ are random variables. To evaluate the coefficients t_i, the following integral is used [10]

$$\begin{aligned} t_i &= \frac{1}{\Psi_i^2} \int_{\Omega} T \Psi_i \left(\xi\right) \rho \left(\xi\right) \mathrm{d}\xi \,, \\ \Psi_i^2 &= \frac{\int \chi \left(\xi\right) \Psi \left(\xi\right) \rho \left(\xi\right) \mathrm{d}\xi}{\int \rho \left(\xi\right) \Psi^2 \left(\xi\right) \mathrm{d}\xi} \,, \end{aligned} \tag{21}$$

where ρ is the PDF of the random variable. The random variable ξ must be transformed into $\chi\left(\xi\right)$ to reflect the space of the probability distribution function. For example, assuming the input parameters are normally distributed and a function of random variables that are also normally distributed with a mean of 0 and standard deviation of 1, the random variable can be scaled as such

$$\begin{aligned} &\xi \sim \mathcal{N}\left(0,1\right) \text{ i.e. } \rho\left(\xi\right) = \frac{1}{\sqrt{2\pi}} \mathrm{e}^{-\frac{\xi^2}{2}} \,, \\ &\chi\left(\xi\right) \sim \mathcal{N}\left(M_N, S_N\right) \,, \\ &\chi\left(\xi\right) = S_N \xi + M_N \,. \end{aligned} \tag{22}$$

In the present study, the input turbulence parameters are defined as polynomials depending on the chosen PDF. Each turbulence parameter can be expressed as a sum of polynomials as follows

$$\begin{aligned} \kappa &= \sum_{i=0}^{\infty} a_i \Psi_{1,i}\left(\xi_1\right) = a_0 \Psi_{1,0}\left(\xi_1\right) + a_1 \Psi_{1,1}\left(\xi_1\right) + a_2 \Psi_{1,2}\left(\xi_1\right) + \dots \,, \\ \varepsilon &= \sum_{j=0}^{\infty} b_j \Psi_{2,j}\left(\xi_2\right) = b_0 \Psi_{2,0}\left(\xi_2\right) + b_1 \Psi_{2,1}\left(\xi_2\right) + b_2 \Psi_{2,2}\left(\xi_2\right) + \dots \,. \end{aligned} \tag{23}$$

The output SPL is also expressed as a sum of polynomials and is orthogonal to the input polynomials

$$\mathrm{SPL}\left(\omega, \boldsymbol{\xi}\right) = \sum_{k=0}^{\infty} c_k\left(\omega\right) \Psi_{3,k}\left(\xi_1, \xi_2\right). \tag{24}$$

Stochastic basis functions are defined based on the chosen PDF to model input variations. For example, with a normal distribution as the stochastic model for the inputs, the stochastic basis functions will be the Hermite polynomials

$$\mathrm{He}_p\left(\xi\right) = (-1)^p \, \mathrm{e}^{\frac{\xi^2}{2}} \frac{\mathrm{d}^p}{\mathrm{d}\xi^p} \mathrm{e}^{-\frac{\xi^2}{2}}. \tag{25}$$

To determine the necessary terms required for the input polynomial expressions, coefficients are evaluated using Eq 21. Coefficients that are close to the value of zero are neglected. The turbulence input polynomial expressions can be sufficiently truncated to the first degree.

$$\kappa = \sum_{i=0}^{1} a_i \mathrm{He}_i\left(\xi_1\right) = a_0 + a_1 \xi_1 \,, \tag{26}$$

$$\varepsilon = \sum_{j=0}^{1} b_j \mathrm{He}_j\left(\xi_2\right) = b_0 + b_1 \xi_2. \tag{27}$$

For the output SPL polynomial, the stochastic basis functions can be calculated using Eq 24 such that the output SPL can be expressed as

$$\begin{aligned} \mathrm{SPL} &= \sum_{k=0}^{9} c_k\left(\omega\right) \Psi_{3,k}\left(\xi_1, \xi_2\right) \\ &= c_0\left(1\right) + c_1\left(\xi_1\right) + c_2\left(\xi_2\right) + c_3\left(\xi_1^2 - 1\right) + c_4\left(\xi_1 \xi_2\right) + c_5\left(\xi_2^2 - 1\right) + \\ &\quad c_6\left(\xi^3 - 3\xi\right) + c_7\left[\left(\xi^2 - 1\right)\xi_2\right] + c_8\left[\xi_1\left(\xi_2^2 - 1\right)\right] + c_9\left(\xi_2^3 - 3\xi_2\right). \end{aligned} \tag{28}$$

Once the coefficients of the input polynomials are determined, the coefficients of the output SPL polynomial are calculated using the stochastic collocation method. The collocation points are chosen to be the roots of the polynomial one order greater than the output polynomial including zero if zero is not already included in the roots. Each turbulence parameter will be set to the corresponding value in each pair of collocation points $\boldsymbol{\xi} = \{\xi_1, \xi_2\}$. In the study, as indicated in Eq 28, third-degree truncation is used for the output polynomial to ensure a converged solution. As such, the roots of the fourth order Hermite polynomial, $\{-1.65, -0.52, 0, 0.52, 1.65\}$, are chosen to be the collocation points as shown in Table 1.

Table 1 Collocation points for PCE output coefficients calculation

1st run ($\boldsymbol{\xi_1}$)	$\xi_{1,1} = -1.65$	$\xi_{1,2} = -1.65$
2nd run ($\boldsymbol{\xi_2}$)	$\xi_{2,1} = -1.65$	$\xi_{2,2} = -0.52$
ith run ($\boldsymbol{\xi_i}$)	$\xi_{i,1} = \ldots$	$\xi_{i,2} = \ldots$
25th run ($\boldsymbol{\xi_{25}}$)	$\xi_{25,1} = 1.65$	$\xi_{25,2} = 1.65$

With these turbulence parameter values, the output SPL is calculated at the collocation points

$$\begin{bmatrix} \mathrm{SPL}_1 \\ \mathrm{SPL}_2 \\ \vdots \\ \mathrm{SPL}_{25} \end{bmatrix} = \begin{bmatrix} \Psi_{3,0}(\boldsymbol{\xi_1}) & \Psi_{3,1}(\boldsymbol{\xi_1}) & \Psi_{3,2}(\boldsymbol{\xi_1}) & \ldots & \Psi_{3,9}(\boldsymbol{\xi_1}) \\ \Psi_{3,0}(\boldsymbol{\xi_2}) & \Psi_{3,1}(\boldsymbol{\xi_2}) & \Psi_{3,2}(\boldsymbol{\xi_2}) & \ldots & \Psi_{3,9}(\boldsymbol{\xi_2}) \\ \vdots & \ldots & \ddots & & \\ \Psi_{3,0}(\boldsymbol{\xi_{25}}) & \Psi_{3,1}(\boldsymbol{\xi_{25}}) & \Psi_{3,2}(\boldsymbol{\xi_{25}}) & \ldots & \Psi_{3,9}(\boldsymbol{\xi_{25}}) \end{bmatrix} \begin{bmatrix} c_0 \\ c_1 \\ \vdots \\ c_9 \end{bmatrix}. \tag{29}$$

Solving the matrix equation for the coefficients of the output polynomial allows the output SPL to be defined as a function of the random variables (See Eq 24). If the input parameters are assumed to be lognormal, a transformation to the normal distribution is required to employ polynomial chaos expansion. A lognormal variable is the exponential of a normal variable (See Eq 18). Taking the exponential of the sampled transformed input parameters will result in a lognormally distributed variable. To contrast this method, a random sampling approach of the Monte Carlo method will also be applied.

2. Random sampling

The Monte Carlo process is a random sampling procedure in which the uncertain input parameters are sampled iteratively from a probability distribution function (PDF) that describes the prescribed stochastic behavior, which includes the mean and variance. The mean of the input parameters T are described by experimental values, which are taken from literature [25]. Variances of the input parameters are then prescribed, and in this case, small values are considered (i.e., CV < 1). Additionally, a prescribed PDF is imposed to describe the statistics of the input parameters. In this study, it is mentioned that the log-normal PDF is motivated to be a suitable candidate for describing the stochastics as mentioned in Kolmogorov's work [31]. The MCS process commences by sampling a very large number of occurrences based on the PDFs. Within each iteration, the output is evaluated. A schematic diagram of this process is illustrated in Figure 2.

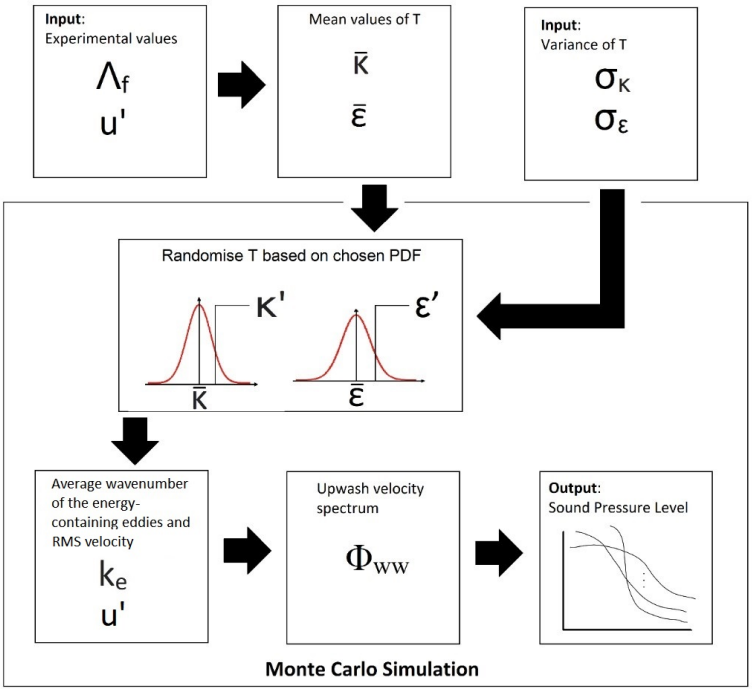

Fig. 2 Schematic of Monte Carlo simulation

III. Results

This section presents results generated from the procedures outlined in the previous Section II. To evaluate the PSD from Eq 1, the integral must be truncated to a sufficient range of spanwise wavenumbers k_y. Therefore in the first part of this section, the cutoff wavenumber necessary to evaluate the integral is estimated by displaying various color maps that represent components of the integrand. Following this are the uncertainty quantification results that are generated using PCE and MCS under various comparisons.

The specifications of the numerical simulation are summarized in Table 2. Turbulence parameters, integral length scale and RMS velocity are obtained from experimental measurements in Santana's work [25]. In Santana's experimental facility, a coarse turbulence generation grid was placed upstream of a NACA-0012 airfoil with 0.1 m chord and 0.2 m span and zero angle-of-attack [25]. Measurements were obtained from a flow speed of 30 $\mathrm{m{\cdot}s^{-1}}$ and 6.35 mm upstream from the leading edge of the airfoil. The numerical simulation assumes the same setup and flow conditions. Thus the experimental values of the turbulence flow parameters are chosen to define the mean values.

Table 2 Specifications of the numerical setup

Parameter	Units	Value
Turbulence integral length scale Λ_f	-	0.0108
Velocity fluctuation root-mean-square u'	$\mathrm{m{\cdot}s^{-1}}$	1.9751
Free stream air speed U_∞	$\mathrm{m{\cdot}s^{-1}}$	30
Airflow density ρ_0	$\mathrm{kg{\cdot}m^{-3}}$	1.225
Speed of sound in air C_∞	$\mathrm{m{\cdot}s^{-1}}$	343
Airfoil semi-chord b	m	0.05
Airfoil semi-span d	m	0.1

The present numerical simulation implements uncertainty quantification by employing Monte Carlo simulation and polynomial chaos expansion to the preliminary results. A convergence study is performed for MCS to determine the number of iterations required for random sampling. The input variations required at which the output SPL uncertainty is consistent when performing various runs are found to be at n = 10000 simulations. Experimental values taken from Santana's study are used to define the mean values of the turbulence parameters, $\bar{T} = \{\bar{\kappa}, \bar{\varepsilon}\}$ and the standard deviation is defined by a CV value. The values of the inputs are varied based on the chosen PDFs. For each iteration, the values For k_e and the velocity fluctuation RMS u' are evaluated to generate an upwash velocity spectrum. Small changes in the upwash velocity spectrum due to variations in the input will alter the output SPL. After n iterations, the output will display n SPL plots and is presented such that the uncertainty can be examined.

A. Cutoff wavenumber estimation

For the numerical evaluation of the integral in Eq 1, a criterion for determining the maximum spanwise wavenumber is required. This is achieved by investigating the integrand, which consists of the modified von Kármán upwash spectrum and aeroacoustic transfer function. Figure 3a shows the map for the modified von Kármán spectrum. It is observed that the values of $\phi_{ww}\left(k_x, k_y\right)$ are negligible for $k_x, k_y > 1000\ \mathrm{m}^{-1}$. Figure 3b shows the color map for the remaining term of the integrand, which includes the following aeroacoustic transfer function

$$H = \pi U d \left(\frac{\rho_0 z k b}{\sigma_0^2}\right)^2 \frac{\sin^2\left[\left(K_y - k_y\right) d\right]}{\pi d \left(K_y - k_y\right)^2} \left|\mathcal{L}\left(x, y, z\right)\right|^2 . \tag{30}$$

A listener position of $(0, 0, 1\ \mathrm{m})$ is chosen. There is a significant contribution from the subcritical gusts up to $K_x = 10^4$. The integrand is then investigated by taking the product of these two functions and normalizing it over each maximum value per K_x in Figure 3c. The Graham's parameter $\left(\Theta = MK_x/\left(\beta k_y\right)\right)$ is also introduced, where less than or greater than unity corresponds to subcritical and supercritical gusts respectively [42]. For a listener position of $(0, 0, 1\ \mathrm{m})$, it is demonstrated that the cut-off spanwise wavenumber is observed to be approximately $k_y^{co} \approx 100\ \mathrm{m}^{-1}$. Beyond this spanwise wavenumber, there is an insignificant contribution from both the subcritical and supercritical gusts. Therefore, it is advised that the integral be evaluated to approximately $1.5k_y^{co} = 150\ \mathrm{m}^{-1}$. The factor of 1.5 is used to ensure that the error of the integral calculation due to the wavenumber domain truncation is minimal.

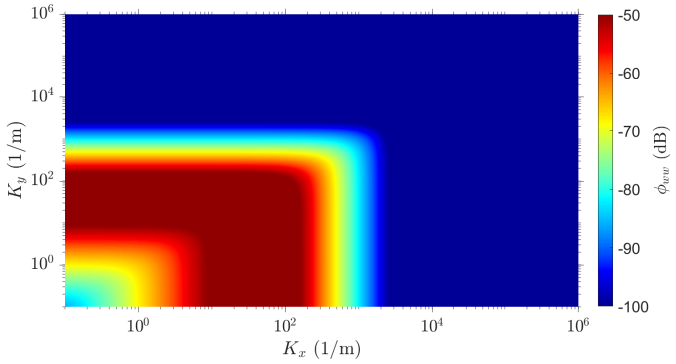

(a)

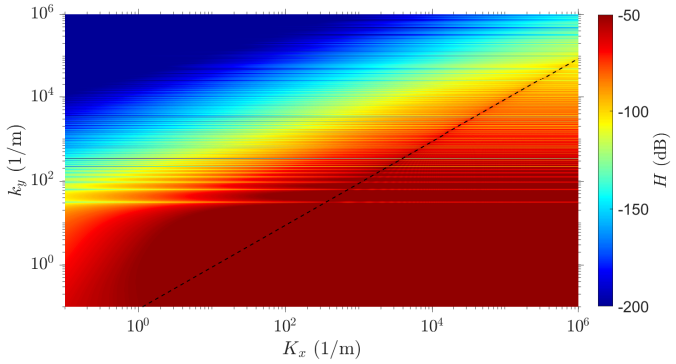

(b)

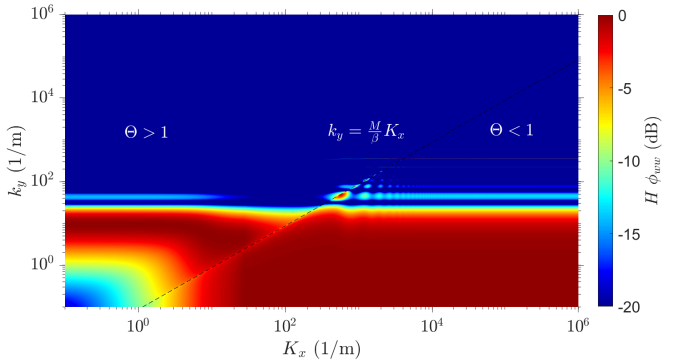

(c)

Fig. 3 Color maps of the (a) von Kármán spectrum (modified under RDT) ϕ_{ww} (dB, reference 1 $\mathrm{m^2 s^{-2} Hz^{-1}}$), (b) H (dB, reference 1 $\mathrm{kg^2 m^{-2} s^{-1}}$), and (c) integrand obtained by the product of (a) and (b), normalized by the maximum value at each convective wavenumber (dB, reference 1 $\mathrm{Pa^2 Hz^{-1}}$). The dashed lines in (b) and (c) correspond to Graham's parameter, showing critical gusts ($\Theta = 1$), which separates subcritical gusts ($\Theta < 1$) from supercritical gusts ($\Theta > 1$).

B. Uncertainty Quantification results

The lognormal distribution and normal distribution are used as two-parameter models for small input variations. Figure 4 presents the output noise levels when describing the input variations using the lognormal distribution, and each turbulence parameter is varied independently while keeping the other at a certain value. The output SPL is determined to converge at third-degree truncation with first-degree truncated input polynomials. From the plots, the turbulence kinetic energy dissipation rate is shown to have a lesser influence on the uncertainty of the output noise levels than the turbulence kinetic energy. Increasing the value of CV for ε from 0.05 to 0.15 results in relatively lower output uncertainty, and for both turbulence parameters, increasing CV results in significant uncertainty introduced to the output noise levels. Figure 5 compares the output generated using a lognormal and normal PDF for the turbulence parameters. Both turbulence parameters are varied simultaneously to observe the effect of the combined uncertainty. The output SPL for normally sampled input parameters is determined to converge at fifth-degree truncation. The results are generally more spread than those generated from a lognormal distribution. Since the normal distribution extends from $(-\infty, \infty)$, it is fundamentally an inaccurate description of the variation in the input turbulence parameters, which are strictly positive. The present study attempts to model input uncertainty under a normal PDF by discarding negative values. When performing multiple runs, using the normal distribution for input variation resulted in less consistent results. More terms are required for the output SPL polynomial to generate an appropriate uncertainty analysis. Using lognormal distribution to model input variation is a more appropriate model for describing the input variation for generating the output uncertainty.

Uncertainty of the output is further explored in Figures 6- 9 using the lognormal distribution for input parameters. The standard deviation of the output SPL is presented in Figure 6. For each turbulence parameter, the CV is set to 0.05, 0.10, and 0.15 while keeping the other parameter certain (CV = 0). The standard deviation of the output SPL is plotted against the Helmholtz number using MCS and PCE. Both UQ methods agree on the standard deviation of the output SPL. The standard deviation increases when a greater CV for the input parameters is used, consistent with the results in Figure 4. The minimum standard deviation correlates to the smallest spread of values in Figure 4. The standard deviation of the output SPL from turbulence kinetic energy variations is greater than turbulence kinetic energy dissipation rate variations. The relationship between the coefficient of variations between the output and input is also investigated. Results generated from variations in turbulence kinetic energy only, turbulence kinetic energy dissipation rate only, and both turbulence kinetic energy and turbulence kinetic energy dissipation rate are presented in Figure 7 for two Helmholtz values, kc = 0.5 and 5, approximately at the two peaks of the mean output SPL. There is a linear relationship presented in the three scenarios where increasing the CV of input is directly proportional to the CV of the output SPL. From the results generated on output SPL uncertainty, there is evidence suggesting significant uncertainty introduced at the output from small input variations. In Figure 8. the probability density functions for the two Helmholtz numbers are estimated. The plots correlate to the distribution of SPL values shown in Figure 4. There is

a greater spread of values for varying the turbulence kinetic energy at $kc = 0.5$ compared to varying the turbulence kinetic energy dissipation rate. The probability density function for the variations in turbulence kinetic energy is flatter and spread across a broader range of SPL values. In contrast, the probability density function for the turbulence kinetic energy dissipation rate is sharply peaked at the mean SPL. At the higher Helmholtz number $kc = 5$, the probability density functions are similar, and there is an insignificant difference between variations in each turbulence parameter. Finally, Figure 9 shows the mean, minimum and maximum predicted SPLs generated by the airfoil under uncertain input parameters at different directions. These directivity plots are presented for two Helmholtz numbers, $kc = 0.5$ and 5 and for combined uncertainties with three different CVs. The envelope of the stochastic response is constructed by calculating the minimum and maximum of all the responses computed by the PCE approach for samples generated by the MCS. It can be seen that the MCS samples are located between the minimum and maximum of the realizations obtained using the PCE method. At low frequencies, the mean value of the predicted SPL is very close to the upper envelope. Moreover, for a given frequency, there is similar uncertainty distribution along the directivity pattern.

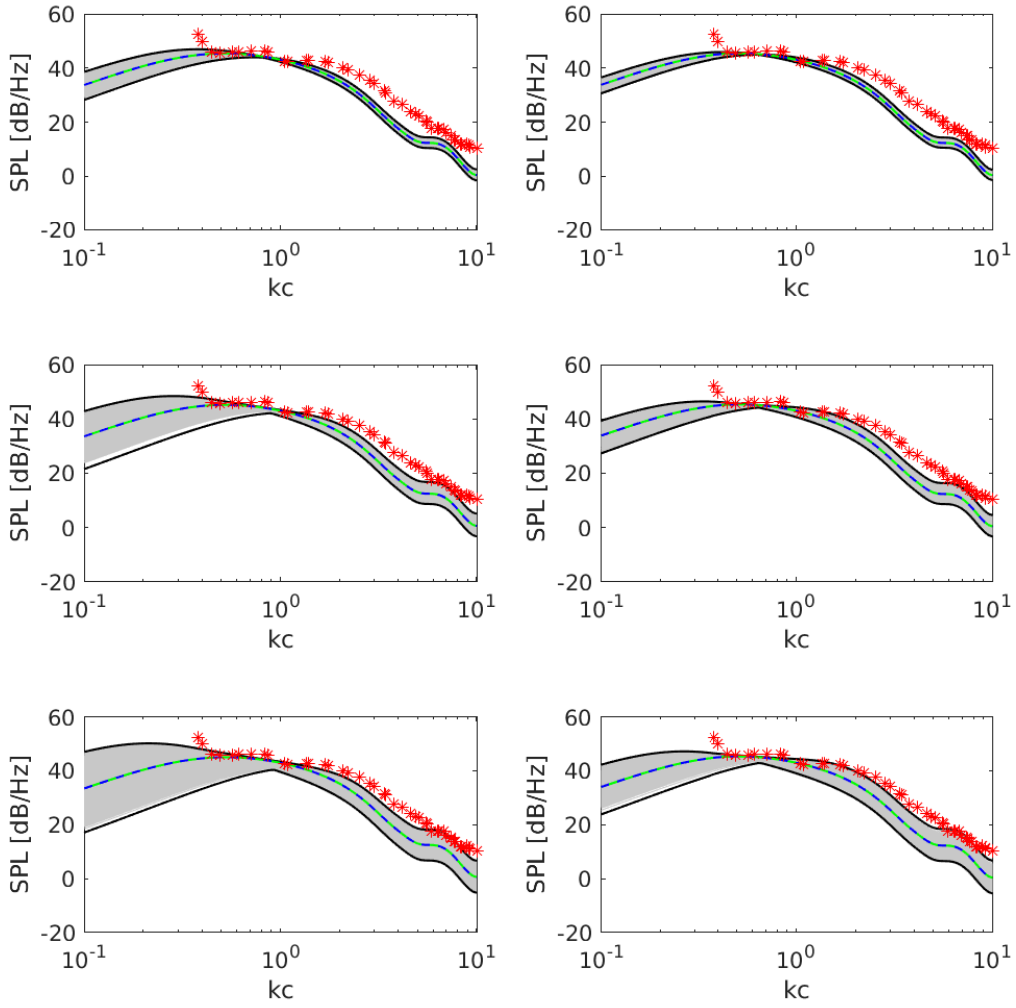

Fig. 4 Output noise uncertainty using lognormal distribution for input variations (n=10000 simulations). A turbulence parameter (κ = Left, ε = Right) is varied at a CV = 0.05 (Top), 0.10 (Middle), and 0.15 (Bottom) while keeping the other parameter certain. Maximum and minimum values from PCE (——); Present mean values from PCE (——); Present mean values from MCS (- - - - -); Present simulated values from MCS (——); Experimental values (*).

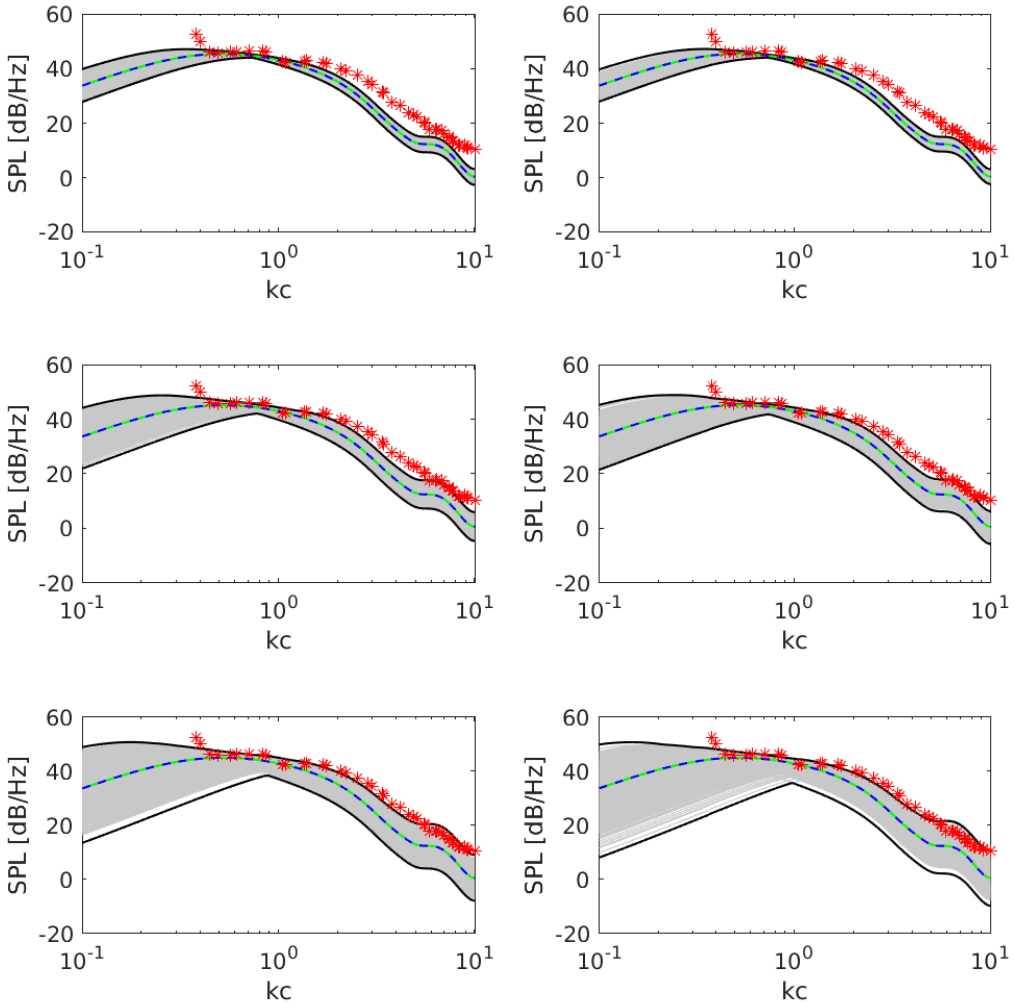

Fig. 5 Comparison of output noise uncertainty using lognormal distribution (Left) and normal distribution (Right) for input variations (n=10000 simulations). Both turbulence parameters are varied at CV = 0.05 (Top), 0.10 (Middle), and 0.15 (Bottom). Maximum and minimum values from PCE (——); Present mean values from PCE (——); Present mean values from MCS (- - - - -); Present simulated values from MCS (——); Experimental values (*).

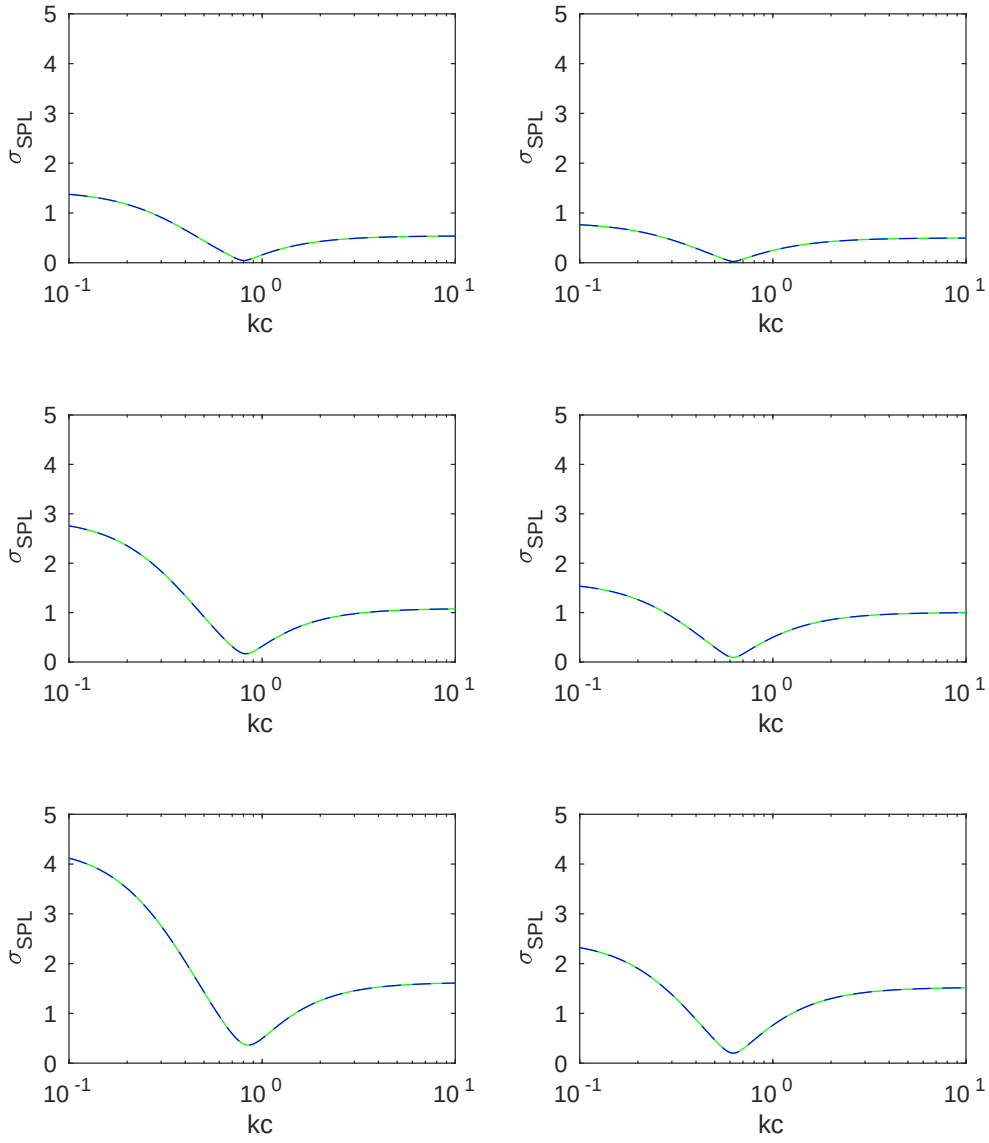

Fig. 6 Standard deviation of the output SPL generated for lognormally distributed input variations (n=10000 simulations) using PCE (——) and MCS (- - - - -). A turbulence parameter (κ = Left, ε = Right) is varied at a CV = 0.05 (Top), 0.10 (Middle), and 0.15 (Bottom) while keeping the other parameter certain.

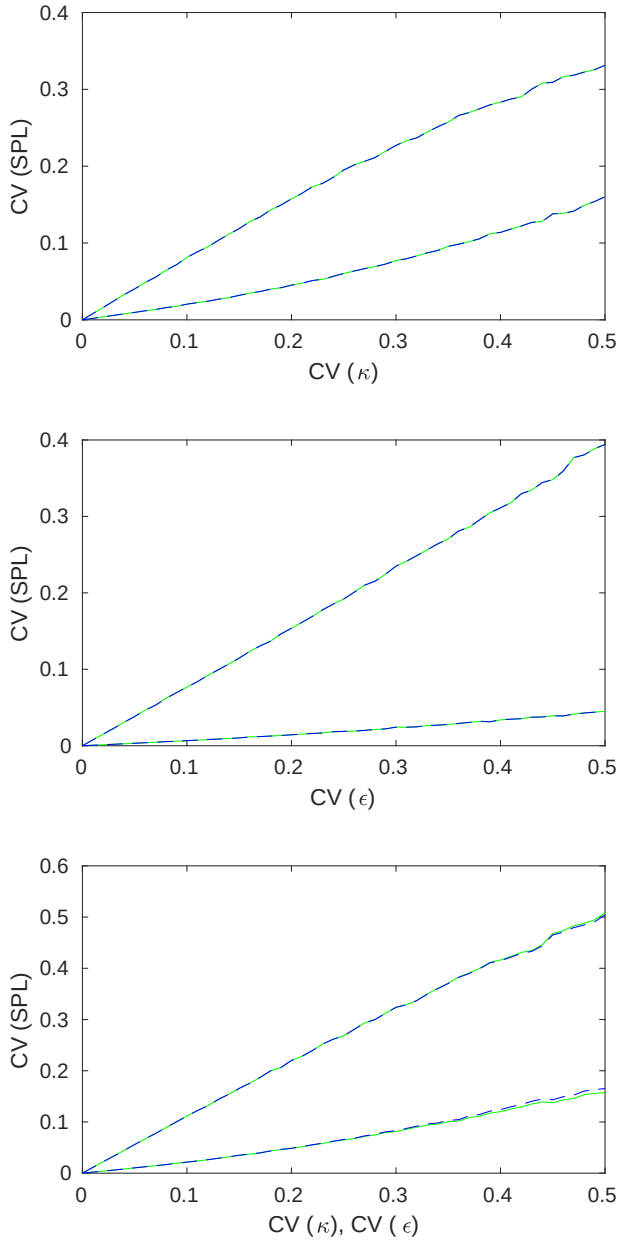

Fig. 7 Relationship between the coefficient of variation of the output and the coefficient of variation of the inputs (Top = κ only; Middle = ε only; Bottom = κ and ε) using PCE (——) and MCS (- - - - -).

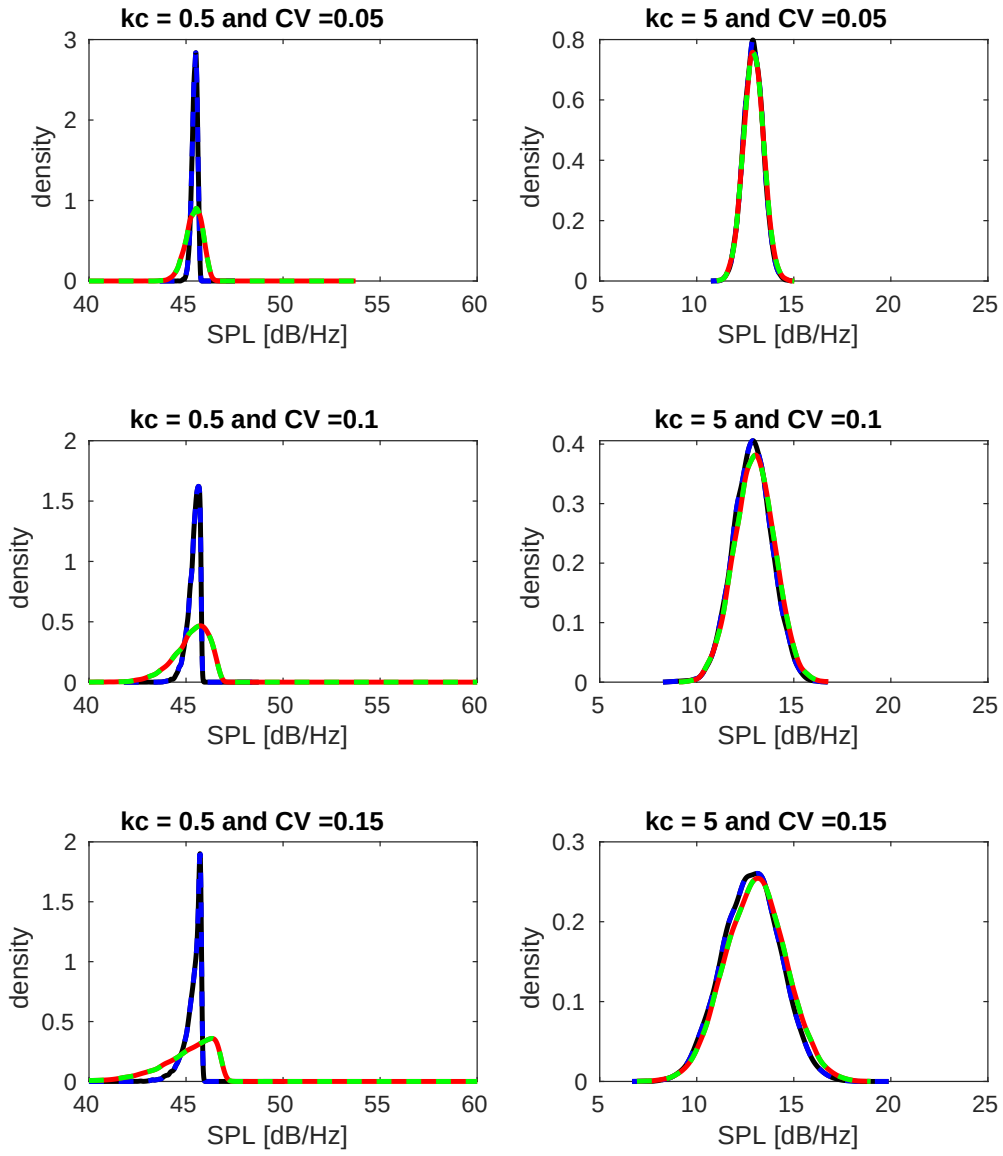

Fig. 8 The approximate probability density function of the SPL at two different frequencies kc = 0.5, 5 by varying κ only and using PCE (——) or MCS (- - - - -); ε only and using PCE (——) and MCS (- - - - -).

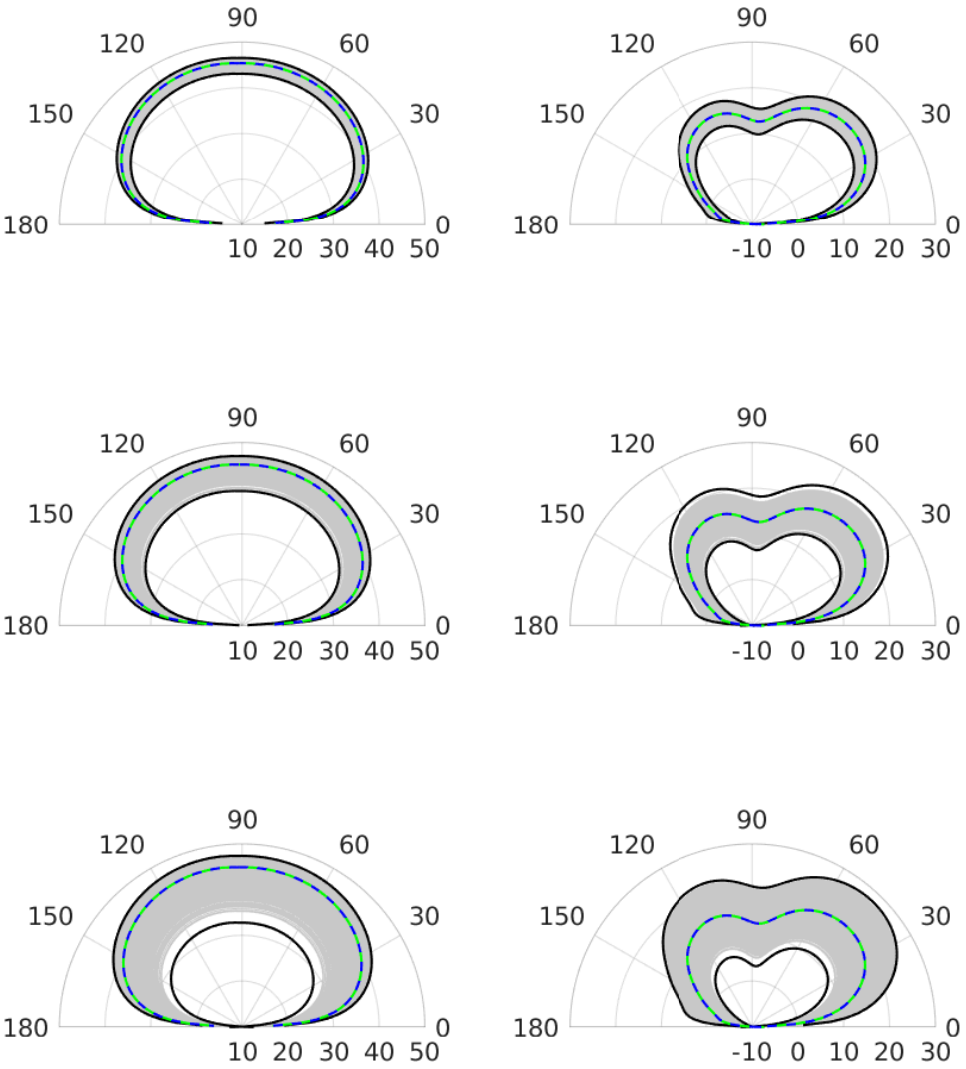

Fig. 9 Directivity patterns in the $x - z$ plane, 1 m from the origin, at two different frequencies kc = 0.5 (Left), 5 (Right) using lognormal distribution for input variations (n=10000 simulations). Both turbulence parameters are varied at CV = 0.05 (Top), 0.10 (Middle), and 0.15 (Bottom). Maximum and minimum values from PCE (——); Present mean values from PCE (——); Present mean values from MCS (- - - - - -); Present simulated values from MCS (——).

It is also worth noting that the computational runtime of PCE is significantly shorter than the runtime for MCS. There is almost negligible runtime difference between the two methods for a low number of iterations $n << 1000$, but PCE becomes more efficient for the converged number of iterations ($n = 10000$). For PCE, only the collocation points must be evaluated to generate the output polynomial, which then can be utilized efficiently for uncertainty analysis. The reason for this difference is due to the protocol of MCS: the output is sampled n times to introduce uncertainty, and this leads to a two-orders-of-magnitude runtime difference between PCE and MCS.

IV. Conclusions

The airfoil-turbulence interaction noise from the leading edge of an airfoil is modeled by Amiet's theory with modifications to the von Kármán upwash velocity spectrum using RDT to better describe the interaction with a turbulent flow. Initially, preliminary results were generated to verify the numerical simulation against Santana's results [25]. Uncertainty quantification was then applied to the numerical simulation, and the variations in uncertain input parameters including the turbulence kinetic energy and its dissipation rate were modeled under various probability distribution functions. PCE was applied to the airfoil-turbulence system, and the uncertainty was compared with results generated from MCS. The uncertainty of the output SPL was further examined regarding variations in standard deviation, CV, probability density functions and directivities. It was found that the lognormal distribution provides the most reasonable and consistent results compared to the normal distribution. The results suggest that there is significant output uncertainty introduced by small variations of the input turbulence parameters. The estimated probability density functions demonstrate that the turbulence kinetic energy can be more uncertain than the turbulence kinetic energy dissipation rate. The PCE method is also recognized to be more computationally efficient compared to MCS. For the numerical simulations, it is observed that there is a factor of two orders of magnitude of time saved in runtime for $n = 10000$ iterations.

Future works can advance this investigation by implementing physically realistic turbulence flow via high-fidelity CFD. The turbulence parameters have been assumed to be independent for stochastic modeling. However, this is likely not the case as the two properties, turbulence kinetic energy and turbulence kinetic energy dissipation rate, are related. The uncertainty analysis can be improved by using a joint distribution and a spatial correlation between turbulence parameters.

References

[1] Liu, W., "A review on wind turbine noise mechanism and de-noising techniques," *Renewable Energy*, Vol. 108, 2017, pp. 311–320. https://doi.org/https://doi.org/10.1016/j.renene.2017.02.034.

[2] Deshmukh, S., Bhattacharya, S., Jain, A., and Paul, A. R., "Wind turbine noise and its mitigation techniques: A review,"

Energy Procedia, Vol. 160, 2019, pp. 633–640. https://doi.org/https://doi.org/10.1016/j.egypro.2019.02.215, 2nd International Conference on Energy and Power, ICEP2018, 13–15 December 2018, Sydney, Australia.

[3] Mahashabde, A., Wolfe, P., Ashok, A., Dorbian, C., He, Q., Fan, A., Lukachko, S., Mozdzanowska, A., Wollersheim, C., Barrett, S. R., Locke, M., and Waitz, I. A., "Assessing the environmental impacts of aircraft noise and emissions," *Progress in Aerospace Sciences*, Vol. 47, No. 1, 2011, pp. 15–52. https://doi.org/https://doi.org/10.1016/j.paerosci.2010.04.003.

[4] Ayton, L. J., and Chaitanya, P., "Analytical and experimental investigation into the effects of leading-edge radius on gust–aerofoil interaction noise," *Journal of Fluid Mechanics*, Vol. 829, 2017, pp. 780–808. https://doi.org/10.1017/jfm.2017.594.

[5] Ayton, L. J., and Kim, J. W., "An Analytic Solution for the Noise Generated by Gust-Aerofoil Interaction for Plates with Serrated Leading Edges," *Journal of Fluid Mechanics*, Vol. 853, 2018, pp. 515–536. https://doi.org/10.1017/jfm.2018.583, arXiv: 1805.05118.

[6] Ayton, L. J., "Analytic solution for aerodynamic noise generated by plates with spanwise-varying trailing edges," *Journal of Fluid Mechanics*, Vol. 849, 2018, pp. 448–466. https://doi.org/10.1017/jfm.2018.431.

[7] Nukala, V. B., and Padhy, C. P., "Concise review: aerodynamic noise prediction methods and mechanisms for wind turbines," *International Journal of Sustainable Energy*, Vol. 42, No. 1, 2023, pp. 128–151. https://doi.org/10.1080/14786451.2023.2168000.

[8] Argyropoulos, C., and Markatos, N., "Recent advances on the numerical modelling of turbulent flows," *Applied Mathematical Modelling*, Vol. 39, No. 2, 2015, pp. 693–732. https://doi.org/https://doi.org/10.1016/j.apm.2014.07.001.

[9] Christophe, J., Moreau, S., Hamman, C. W., Witteveen, J. A. S., and Iaccarino, G., "Uncertainty Quantification for the Trailing-Edge Noise of a Controlled-Diffusion Airfoil," *AIAA Journal*, Vol. 53, No. 1, 2015, pp. 42–54. https://doi.org/10.2514/1.J051696.

[10] Sepahvand, K., Marburg, S., and Hardtke, H.-J., "Uncertainty Quantification in Stochastic Systems Using Polynomial Chaos Expansion," *International Journal of Applied Mechanics*, Vol. 02, No. 02, 2010, pp. 305–353. https://doi.org/10.1142/S1758825110000524.

[11] Mosleh, A., Sepahvand, K., Varum, H., Jara, J., Razzaghi, M. S., and Marburg, S., "Stochastic collocation-based nonlinear analysis of concrete bridges with uncertain parameters," *Structure and Infrastructure Engineering*, Vol. 14, No. 10, 2018, pp. 1324–1338. https://doi.org/10.1080/15732479.2018.1434209.

[12] Mazzoni, C. M., Ahlfeld, R., Rosic, B., and Montomoli, F., "Uncertainty Quantification of Leakages in a Multistage Simulation and Comparison With Experiments," *Journal of Fluids Engineering*, Vol. 140, No. 2, 2018, p. 021110. https://doi.org/10.1115/1.4037983.

[13] DeGennaro, A. M., Rowley, C. W., and Martinelli, L., "Uncertainty Quantification for Airfoil Icing Using Polynomial Chaos Expansions," *Journal of Aircraft*, Vol. 52, No. 5, 2015, pp. 1404–1411. https://doi.org/10.2514/1.C032698.

[14] Datz, J., Karimi, M., and Marburg, S., "Effect of Uncertainty in the Balancing Weights on the Vibration Response of a High-Speed Rotor," *Journal of Vibration and Acoustics*, Vol. 143, No. 6, 2021, p. 061002. https://doi.org/10.1115/1.4049628.

[15] Wang, L., Zhou, Z., and Liu, J., "Interval-based optimal trajectory tracking control method for manipulators with clearance considering time-dependent reliability constraints," *Aerospace Science and Technology*, Vol. 128, 2022, p. 107745. https://doi.org/https://doi.org/10.1016/j.ast.2022.107745.

[16] Liu, J., and Wang, L., "Two-stage vibration-suppression framework for optimal robust placements design and reliable PID gains design via set-crossing theory and artificial neural network," *Reliability Engineering & System Safety*, Vol. 230, 2023, p. 108956. https://doi.org/https://doi.org/10.1016/j.ress.2022.108956.

[17] Wang, L., Liu, J., Zhou, Z., and Li, Y., "A two-stage dimension-reduced dynamic reliability evaluation (TD-DRE) method for vibration control structures based on interval collocation and narrow bounds theories," *ISA Transactions*, Vol. 136, 2023, pp. 622–639. https://doi.org/https://doi.org/10.1016/j.isatra.2022.10.033.

[18] Wang, L., Zhao, Y., Liu, J., and Zhou, Z., "Uncertainty-oriented optimal PID control design framework for piezoelectric structures based on subinterval dimension-wise method (SDWM) and non-probabilistic time-dependent reliability (NTDR) analysis," *Journal of Sound and Vibration*, Vol. 549, 2023, p. 117588. https://doi.org/https://doi.org/10.1016/j.jsv.2023.117588.

[19] Gotoh, T., and Kraichnan, R. H., "Turbulence and Tsallis statistics," *Physica D: Nonlinear Phenomena*, Vol. 193, No. 1-4, 2004, pp. 231–244. https://doi.org/10.1016/j.physd.2004.01.034.

[20] Lohse, D., and Grossmann, S., "Intermittency in turbulence," *Physics A 194*, 1993, pp. 519–531.

[21] Frisch, U., *Turbulence: the legacy of A.N. Kolmogorov*, Cambridge University Press, 1995.

[22] Amiet, R. K., "Acoustic radiation from an airfoil in a turbulent stream," *Journal of Sound and Vibration*, Vol. 41, No. 4, 1975, pp. 407–420.

[23] Curle, N., "The influence of solid boundaries upon aerodynamic sound," *Proceedings of the Royal Society of London*, 1955, pp. 505–514.

[24] Moreau, S., and Roger, M., "Back-scattering correction and further extensions of Amiet's trailing-edge noise model. Part II: Application," *Journal of Sound and Vibration*, Vol. 323, No. 1-2, 2009, pp. 397–425. https://doi.org/10.1016/j.jsv.2008.11.051.

[25] Santana, L. D., Christophe, J., Schram, C., and Desmet, W., "A Rapid Distortion Theory modified turbulence spectra for semi-analytical airfoil noise prediction," *Journal of Sound and Vibration*, Vol. 383, 2016, pp. 349–363. https://doi.org/10.1016/j.jsv.2016.07.026.

[26] Najm, H. N., "Uncertainty Quantification and Polynomial Chaos Techniques in Computational Fluid Dynamics," *Annual Review of Fluid Mechanics*, Vol. 41, No. 1, 2009, pp. 35–52. https://doi.org/10.1146/annurev.fluid.010908.165248.

[27] Hariri-Ardebili, M. A., and Sudret, B., "Polynomial chaos expansion for uncertainty quantification of dam engineering problems," *Engineering Structures*, Vol. 203, 2020, p. 109631. https://doi.org/https://doi.org/10.1016/j.engstruct.2019.109631.

[28] Shen, D., Wu, H., Xia, B., and Gan, D., "Polynomial Chaos Expansion for Parametric Problems in Engineering Systems: A Review," *IEEE Systems Journal*, Vol. 14, No. 3, 2020, pp. 4500–4514. https://doi.org/10.1109/JSYST.2019.2957664.

[29] Sepahvand, K., Marburg, S., and Hardtke, H.-J., "Uncertainty quantification in stochastic systems using polynomial chaos expansion," *International Journal of Applied Mechanics*, Vol. 02, No. 02, 2010, pp. 305–353. https://doi.org/10.1142/S1758825110000524.

[30] Walters, G., "Application of generalized polynomial chaos to flow-induced vibration and sound," Ph.D. thesis, The Pennsylvania State University, Dec. 2020.

[31] Kolmogorov, A. N., "A refinement of previous hypotheses concerning the local structure of turbulence in a viscous incompressible fluid at high Reynolds number." *Journal of Fluid Mechanics*, Vol. 13, No. 1, 1962, pp. 82–85.

[32] Kucukcoskun, K., Christophe, J., Schram, C., Anthoine, J., and Tournour, M., "An Extension of Amiet's Theory for Spanwise-Varying Incident Turbulence and Broadband Noise Scattering Using a Boundary Element Method," 2010.

[33] de Santana, L., "Semi-analytical methodologies for airfoil noise prediction," *Arnberg Doctoral School, KU Leuven*, 2015.

[34] Christophe, J., "Application of hybrid methods to high frequency aeroacoustics," *Université Libre de Bruxelles*, 2011.

[35] Rozenberg, Y., "Modélisation analytique du bruit aérodynamique à large bande des machines tournantes: utilisation de calculs moyennés de mécanique des fluides," *Ecole Centrale de Lyon, Lyon, France*, 2007.

[36] Abramowitz, M., and Stegun, I. A., "Handbook of mathematical functions," *Dover Publications, New York*, 1970.

[37] Al Am, J., Clair, V., Giauque, A., Boudet, J., and Gea-Aguilera, F., "Direct noise predictions of fan broadband noise using LES and analytical models," *28th AIAA/CEAS Aeroacoustics 2022 Conference*, 2022, p. 2882.

[38] Bowen, L., Celik, A., and Azarpeyvand, M., "A thorough experimental investigation on airfoil turbulence interaction noise," *Physics of Fluids*, Vol. 35, No. 3, 2023.

[39] Hinze, J. O., *Turbulence*, second edition ed., McGraw-Hill, 1975.

[40] Hunt, J. C. R., "A theory of turbulent flow round two-dimensional bluff bodies," *Journal of Fluid Mechanics*, Vol. 61, No. 4, 1973, pp. 625–706. https://doi.org/10.1017/S0022112073000893.

[41] Batchelor, G. K., and Proudman, I., "The effect of rapid distortion of a fluid in turbulent motion," *The Quarterly Journal of Mechanics and Applied Mathematics 7*, 1954, pp. 83–103.

[42] Karimi, M., Croaker, P., Skvortsov, A., Maxit, L., and Kirby, R., "Simulation of airfoil surface pressure due to incident turbulence using realizations of uncorrelated wall plane waves," *The Journal of the Acoustical Society of America*, Vol. 149, No. 2, 2021, pp. 1085–1096. https://doi.org/10.1121/10.0003498.